Hindawi
Mathematical Problems in Engineering
Volume 2019, Article ID 1414872, 10 pages
https://doi.org/10.1155/2019/1414872

Research Article

Analysis on Vibration Characteristics of Air Film Damping with Open Boundaries

Hong Zhang, Dong-ze Cui, Ying-jie Jiao, and Xi Chen

Sino-European Institute of Aviation Engineering, Civil Aviation University of China, Tianjin 300300, China

Correspondence should be addressed to Dong-ze Cui; 85467710@qq.com

Received 30 January 2019; Accepted 18 March 2019; Published 2 April 2019

Academic Editor: Francesco Tornabene

Air film damping (AFD) has been a research focus for the fatigue damage suppression problem of aeroengine blade decades ago; however significant progress has not been made in the past decade. In this paper, we present a theoretical model and experimental analysis about this technology. The dissipation mechanism of the AFD is established by assumption that the viscous gas inside the thin air film is Poiseuille flow and the energy dissipation equation of AFD with open boundaries is deduced and evaluated. Blade simulated testing specimens are designed. The vibration measurements are performed by RC-3000 vibration exciter and detected by applying the contactless laser vibrometer system. The theoretical results consist with the experimental results, and both show that AFD appears promising performance in vibration suppression. We also present how the structure parameters, such as installation position, air film length and thickness, and thin skin thickness, influence the vibration suppression effect.

1. Introduction

The vibration is the most important reason of aeroengine structural failure. According to the statistics from the aeroengine design manual [1], the faults caused by vibration account for more than 60% of the total engine faults, and the faults caused by blade vibration account for more than 70% of the total vibration faults. Therefore, the blades must be designed to sustain the vibration fatigue damage, thus effectively prolonging the maintenance cycle and reducing the maintenance cost of aeroengine.

There are hitherto four damping technologies which can effectively suppress the blade vibration [2], namely, dry friction damping, constraint layer damping, shock damping, and AFD. Among them, dry friction damping and constrained layer damping are traditional passive damping technologies and have been widely applied. However, dry friction damping is merely applicable for low frequency vibration machinery and the constrained layer damping cannot withstand high centrifugal load which means it cannot be applied to high-speed rotor blades. Shock damping and AFD are semiactive damping methods [2, 3]. Shock damping has a complex mechanism of vibration suppression and is not easy to implement [3], while AFD has a simple structure and is easy to manufacture. In addition, AFD can effectively suppress vibration in a wide frequency range [2]. Therefore, AFD has a more extensive application prospect relative to others in aeroengine blade vibration suppression.

The structure of AFD system includes a plate, a thin skin, and an air film trapped in between. When the AFD structure is subjected to external excitation, the thin skin vibrates asynchronously to the plate due to its different structural parameters. The viscous air in the film will be drived to "pump in and out" by plate and the thin skin. If this behavior occurs in different regions of the air film, that is AFD with sealed boundaries. If this behavior occurs between the air film and the external atmosphere, that is AFD with open boundaries. The vibration energy is then transferred from the solid to the fluid and dissipated by means of fluid motion. On the other hand, the vibration energy is dissipated due to the boundary layer or viscous shear stress in the air film. Due to the complexity in analysis of AFD with open boundaries, there was less significant progress in the past decade.

The importance of AFD was first made clear by the experiments carried out by Ungar [4], and the subsequent explanation was provided by Maidanik [5] in which the viscous losses in the air film by the vibration of the AFD structure are investigated. Since then, several researchers

have investigated AFD technology. Fox [6] established a theoretical model of AFD vibration characteristics based on the linear plane beam theory and verified the method by the experiments. Chow [7, 8] considered the case of straight-crested waves in a plate of infinite extent. In his analysis, the thin skin was treated simply as an additional mass, and the inertia of the fluid could be ignored for thin air film at low frequency. Trochidis [9] has developed a theoretical analysis with the assumption that the gas in the air film is incompressible. And the influence of boundary layer can be neglected in his model because the air film thickness is much thicker than the boundary layer. Lewis [2, 10–13] designed an AFD structure sealed in the turbine fan blade and then carried out the calculation by applying the finite element analysis software. Peter J. Torvik [14] established a simplified model of the AFD structure based on the plate vibration theory and studied the energy dissipation of the AFD structure; based on this theoretical model, Zhang Dayi [15] has validated the influence of structural parameters on the performance of AFD by numerical calculation. Mathison [16] applied gauges to capture vibration signals of AFD structure at different atmospheric pressures in experiments. The application of gauges on the plate will change the original structure of AFD system, so the results need modification to eliminate the error.

The motion of the viscous fluid inside the air film is the key for AFD; therefore it is essential to establish a precise model of fluid motion for understanding the mechanism of vibration energy dissipation. However, former researchers have idealized the fluid motion to simplify the theoretical model. In view of the deficiencies in the previous theoretical analysis and experimental measurements, a theoretical model of the fluid motion is presented by the assumption that the air flow inside the air film is viscous Poiseuille flow in this paper. The energy dissipation equation of AFD with open boundaries is deduced and evaluated. The experiments are conducted with laser vibrometer in order to reduce the measurement error [17]. The aim of this investigation is to develop theoretical analysis methods of AFD by experiment verification and analyze the effects of AFD structure parameters on the damping effect for its future application.

2. Theoretical Analysis

2.1. The Motion Characteristics of the Fluid. The schematic diagram of the side view and front view of the plate with AFD is shown as Figure 1.

2L, *2d,* and *H* represent the length, width, and thickness of the plate, respectively, and *h* represents the thickness of the air film. The coordinate system is set up in the center of the air film, and the *z*-axis is set vertically upward according to the right-hand rule.

Assuming that the vibration mode of the thin skin relative to the plate is (*n, m*), the change of air film thickness caused by the asynchronous vibration of the plate and thin skin is

$$D_{nm}(x, y, t) = D_{0nm} \sin\left(\frac{n\pi x}{2l}\right) \cos\left(\frac{m\pi y}{2d}\right) \sin(\omega t) \quad (1)$$

where D_{0nm} is the thickness of the air film in steady state; *2l* and *2d* are the length and width of the air film, respectively; ω is the vibration frequency of the plate.

A reference system inside the air film is necessary in order to derive the volumetric flow rate equation of the fluid in the air film; therefore, the fluid between the *xoz* plane and the parallel plane with a distance *dy* is considered as the control body for further analysis. This control body is shown in Figure 2.

Since the air film is open at the opposite boundaries, the flow direction is dominated to the transverse direction [8]; thus the fluid is assumed to flow along the *y*-axis. The volumetric flow rate equation is

$$\Delta U = dxdy\,\dot{D} = dxdyD(x, y, t)\,\omega \cot \omega t \quad (2)$$

where $\dot{D}$ represents the time-derivative function of $D(x, y, t)$.

Consider the continuity function of the fluid in the air film; the volumetric flow rate at a random point x in the control body is

$$U(x, y, t) = D_0 \sin\left(\frac{\pi y}{2d}\right) dy \frac{l}{\pi} \left[1 - \cos\left(\frac{\pi x}{l}\right)\right] \omega \cot \omega t \quad (3)$$

Assuming that the fluid is Poiseuille fluid [14], the velocity distribution of fluid in the *z*-axis is parabolic; in this circumstance, another calculation method of fluid volume flow rate at a given vibration frequency ω should be

$$U(x, y, t) = dx \int_0^h v(x, y, z, t)\, dz \quad (4)$$

where $v(x, y, z, t)$ is the velocity equation of fluid in air film.

In the control body shown in Figure 2, the volume flow rate equation can be deduced by integrating the velocity of the fluid along the distance traveled by fluid. Therefore, the velocity equation (5) can be derived by dividing the volumetric flow rate equation from the cross section of the fluid flow,

$$v(x, y, z, t) = \frac{3\omega D_0}{2h} y \sin\left(\frac{\pi x}{2l}\right) \frac{hz - z^2}{(h/2)^2} \cot(\omega t) \quad (5)$$

The velocity and pressure of the fluid can be correlated by momentum conservation equation; the complex stiffness method [6] is introduced to derive the linear form of momentum conservation equation as shown in equation (6):

$$\mu \frac{\partial^2 v(x, y, z)\, e^{j\omega t}}{\partial z^2} - j\omega\rho_0 v(x, y, z) = \frac{\partial P(x, y, z)}{\partial z} \quad (6)$$

where μ is fluid viscosity, ρ_0 is initial density of the fluid, and P is the complex amplitude of fluid pressure.

It is assumed that the fluid is in adiabatic state, e.g., $P/P_0 = \gamma\rho/\rho_0$, where γ is the specific heat capacity of the fluid. Considering the continuity equation of the fluid [13], the pressure distribution equation (7) is

$$\Delta P + \frac{\rho_0\omega^2}{\gamma P_0} \frac{P}{K(\kappa h/2)} = \frac{\rho_0}{K(\kappa h/2)} \frac{D(x, y, t)}{h} \quad (7)$$

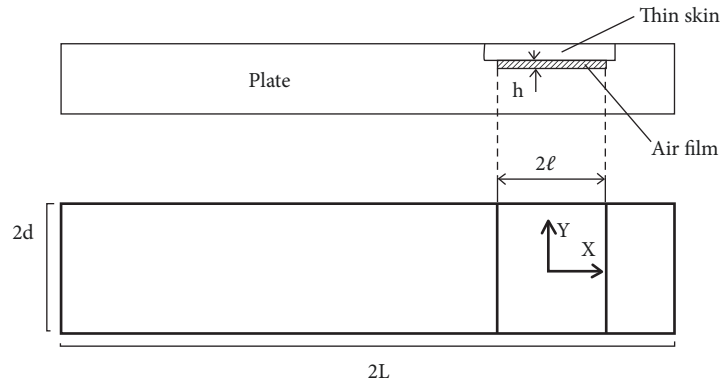

Figure 1: Side view and front view of the plate with AFD.

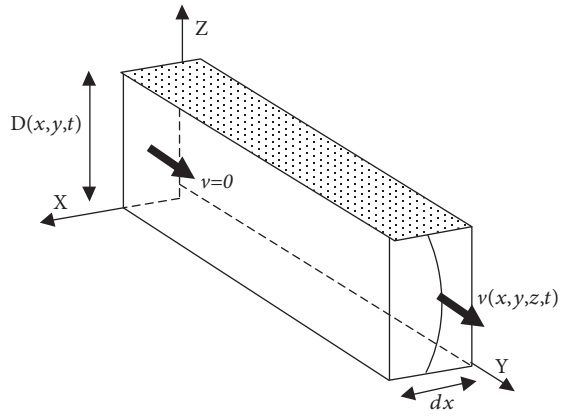

Figure 2: Control body of the fluid in the air film.

where

$$K\left(\frac{\kappa h}{2}\right) = \left[1 - \frac{\tan(\kappa h/2)}{\kappa h/2}\right] \tag{8}$$

$\kappa = -j\rho_0\omega/\mu$ is named the complex viscosity equation of the fluid.

The pressure distribution equation of the fluid is solved as follows:

$$P(y) = \frac{\gamma\rho_0}{\left[\gamma P_0 {r_n}^2 K(\kappa h/2)/\rho_0\omega^2 - 1\right]}\left(\frac{\cos q_n y}{\cos q_n d} - 1\right)\frac{D_0}{h} \tag{9}$$

Among them, q_n is the formation wave number [18] in y-axis of the control body:

$${q_n}^2 = \left[{r_n}^2 - \frac{\rho_0\omega^2}{\gamma P_0 K(\kappa h/2)}\right] \tag{10}$$

r_n is the n^{th} positive roots of equation $\cos(r_n l)\cosh(r_n l) = 1$.

2.2. Energy Dissipation in AFD System. In order to verify the theoretical model of the fluid in the AFD system, the simplified solution of equation (9) is

$$\begin{aligned} P(y) &= \frac{\gamma\rho_0}{\left[\gamma P_0 {r_n}^2 K(\kappa h/2)/\rho_0\omega^2 - 1\right]}\left(\frac{\cos q_n y}{\cos q_n d} - 1\right)\frac{D_0}{h} \\ &\equiv \left[R(\omega) + jI(\omega)\right] D_0 \cos\left(r_n x\right) \end{aligned} \tag{11}$$

In the AFD structure, the energy dissipated in each vibration period equals the integral of the product of pressure and velocity [19], as shown in equation (12):

$$C = \pi \iint_{AREA} \Im\{PD\} = \pi {D_0}^2 I(\omega)\left[1 + \frac{\sin 2r_n l}{2r_n l}\right] 2dl \tag{12}$$

Equation (12) is in agreement with the classical fluid-solid coupling theory [6]: the energy dissipation of the fluid in a rectangular thin cavity originates from the imaginary part of the fluid pressure.

For facilitating the numerical calculation of the AFD structure and the comparison with the previous results [6, 12], the damping ratio, η_{sys}, is defined as the ratio of energy lost

from the system per cycle of oscillation to 2π times the maximum strain energy of the system,

$$\begin{aligned} U_S &= \iint_{AREA} \frac{E}{2}\left(\frac{\partial^2 D}{\partial x^2}\right) dA \\ &= \int_{-l/2}^{l/2}\int_{-b/2}^{b/2} \frac{1}{2}\frac{EH^3 r_n^4}{12} D_0^2 \sin^2\left(r_n x\right) dxdy \\ &= \frac{1}{2}\frac{EH^3 r_n^4}{12}\frac{bl}{2} D_0^2 \end{aligned} \tag{13}$$

$$\begin{aligned} U_A &= \iint_{AREA} \frac{R(\omega)}{2} D(x,y)^2 dA \\ &= R(\omega) D_0 2dl\left[1 + \frac{\sin 2r_n l}{2r_n l}\right] \end{aligned} \tag{14}$$

$$\eta_{SYS} = \frac{1}{2\pi}\frac{C}{U_S + U_A} = \frac{I(\omega)}{Eh^3 {r_n}^4/12 + R(\omega)} \tag{15}$$

where U_S is the strain energy of the plate, U_A is the energy of the gas stored in the air film, and E is Young's modulus.

From equations (12) to (15), it is evident that the vibration suppression effect of the AFD structure depends on the following parameters:

(1) The pressure of the fluid in the film, the specific heat capacity γ of the fluid

(2) The vibration frequency ω of the plate, the wave number q_n(3) The structural parameters of the air film, such as length, width, and thickness

3. Experimental Analysis

In the analysis of AFD, the theoretical calculation and experimental analysis are of equal significance. However, the theoretical model is derived by idealizing the fluid motion which leads to deviation from the actual situation; we can get much closer to the actual situations by carrying out the vibration experiment which aims to compare the theoretical results with the experimental ones.

3.1. Experimental Equipment. The manufactured AFD plates are shown in Figure 3. According to Figures 1 and 3, the manufacturing method of AFD is as follows: a first shallow groove is milled in the plate, a second groove is milled in the first one, then cover a thin skin whose thickness equals the depth of the first groove, an air film is then left in between, and the boundaries of the AFD are left open to the atmosphere.

In order to analyze the vibration suppression effect of the AFD structure with efficiency, plate specimens with different installation positions and structural parameters were designed according to the fan blades.

In order to simulate the damping of AFD on aeroengine blade, TC-4 titanium alloy is used as raw material. All the necessary parameters are shown in Table 1.

Mathison et al. [16] studied the case of AFD plates with sealed boundaries; they carried out vibration experiments by attaching strain gauges to the plates and then compared the vibration response of solid plate with AFD plates and achieved intriguing findings. However, the attached strain gauges change the original structure of the plate specimens and lead to measurement error. In order to reduce the error, RC-3000 vibration testing system is selected as the excitation platform and contactless laser vibrometer system is applied to measure and record the vibration response of plate specimens. The equipment is shown in Figure 4.

Aluminium alloy fixture is chosen to improve the test efficiency since it is of good stability and it can be conveniently installed and removed. In addition, the resonance frequency of the specially designed aluminum alloy fixture is 4475.6 *Hz*, which is far greater than the measured resonance frequency of the plate specimens; therefore the measurement accuracy stays high [20]. During each test, the resonance modes of the plate specimens were measured at first, and the frequency step is then set to 0.5 *Hz* near the resonance band, while the frequency step is set to 2 *Hz* outside the resonance band for convenience of experiment. To improve the accuracy of vibration measurement, contactless laser vibrometer system is applied since no sensor is attached with the plate specimens thus eliminating structural change of the AFD structure. According to the simulation results in finite element analysis, the vibration suppression effect of the AFD is obvious within its first several resonant modes [14]; therefore this experiment is carried out below 500 *Hz* as measurements in higher frequency range may boost the error of feedback signal, and the thin skin might bounce and then collides with nearby equipment or the operators.

4. Data Comparison and Analysis

The original experimental data is barely electronic feedbacks measured by contactless laser vibrometer system; it is transferred by a FFT algorithm to obtain the amplitude-frequency information for further research. The experimental results of solid plate specimen indicate that the frequencies of its first two naturals are 59.7 *Hz* and 379 *Hz*, respectively. Note that the frequency ratio is the ratio of the resonance frequency of each AFD plate to the first-order resonance frequency of the solid plate; necessary parameters such as error and vibration suppression rate are calculated according to equation (16):

$$error = \left|1 - \frac{\text{theoretical result}}{\text{experimental result}}\right| \times 100\% \tag{16}$$

4.1. Vibration Damping Effect of AFD. Experimental results show that AFD can effectively suppress plate vibration; Figure 5 shows the damping effect of AFD in different resonance frequency bands; the detailed vibration information is shown in Table 2.

From Figure 5 and Table 2, it is found that, in first two vibration modes (0-100 *Hz*; 350-450 *Hz*), AFD can significantly suppress the plate vibration. The resonance bands of the solid plate measured by theoretical calculation and experiment are close; the maximum error between the theoretical results and the experimental results is 6.75%, which indicates that the theory considering fluid motion in the air film has good solution precision [16]. Therefore, the

Table 1: Properties of plates.

Property	Symbol	Value[Unit]
Plate length	$2L$	300[mm]
Plate width/Air film width	$2D$	100[mm]
Plate thickness	H	7.5[mm]
Air film length	$2l$	- - - -
Air film thickness	h	- - - -
Density	ρ	4500[kg/m^3]
Young's modulus	E	$1.1*10^{11}$[Pa]
Absolute viscosity	μ	$1.81*10^{-5}$[Pa.S]

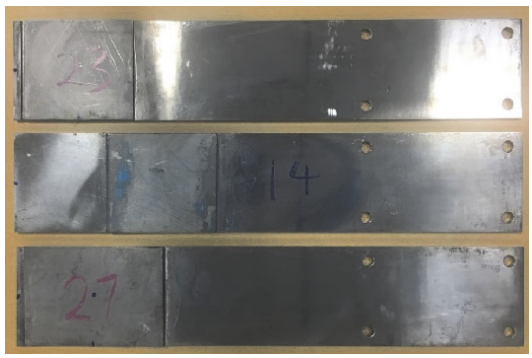

Figure 3: Plate specimens with AFD system.

theoretical model of the AFD system deduced in this paper is worth further research.

4.2. Effect of Installation Positions on AFD. The air film in the AFD plate is 1.5 *mm* thick; acceleration of the vibration excitation is set to 20 m/s^2 at ambient pressure P_0=101.3 *kPa*. The different installations of thin skin are shown in Figure 6(a), and the vibration information is shown in Figure 6(b). Comparison of vibration frequency-amplitude is shown in Table 3.

4.3. Effect of Air Film Length on AFD. From equation (12), it is trivial that the air film length is one of the key parameters that influence the vibration suppression effect of AFD. In order to quantify this influence, the AFD structure is designed as follows: thin skin is installed in Position 1 as illustrated in Figure 6(a), air film is 1.5 *mm* thick, and the air film lengths are 60 *mm*, 80 *mm*, and 100 *mm*, respectively; the acceleration of the vibration excitation is set to 20 m/s^2 in the experiments. The vibration information is shown in Figure 7 and Table 4.

As shown in Figure 7, the change of air film length leads to an increase of the resonance frequency of the AFD plate, and the resonance frequency increases as the air film length becomes larger.

From Table 4, the minimum vibration suppression rate of AFD plates is 55.782%, indicating that the AFD structure with different air film lengths can all effectively suppress the vibration; however the vibration suppression effect is the best when air film length is 80 *mm*, and its vibration suppression effect will be weakened when air film is either too thick or too thin; this indicates that the air film has an optimal thickness to meet the best damping performance. The air film length must be determined according to the structure of aeroengine fan blades in order to achieve the best vibration suppression performance.

5. Results Comparison

From equations (12) to (15), it is evident that the vibration suppression effect of the AFD structure depends on the structure parameters of air film and thin skin; the theoretical damping ratio is calculated by MATLAB; the experimental damping ratio is calculated by vibration response of AFD plate specimens.

5.1. Effect of Air Film Thickness on Damping Ratio. The AFD system with open boundaries is connected with external atmosphere; in this case, the initial pressure in the air film is P_0=101.3 *kPa*. The AFD is installed in Position 1 and the air film length is designed as 80 *mm*, and the air film thickness varies from 0.125 *mm* to 1 *mm*. The damping ratio of AFD at different air film thickness is shown in Figure 8. It is found that the damping ratio decreases logarithmically as the air film thickness increases logarithmically. This phenomenon is trivial to explain: with the increase of air film thickness, the asynchronous vibration of the plate specimen and thin skin is weakened which reduces the viscous loss of vibration energy, thus resulting in the decrease of damping ratio.

Since the coordinates of Figure 8 are logarithmic, the difference between theoretical data and experimental data is not obvious; the theoretical damping ratio is therefore compared with the experimental damping ratio in Table 5.

The Levenberg-Marquardt algorithm [21] is applied for the nonlinear fitting of the data in Table 5. It is found that the relationship between damping ratio and air film thickness conforms to equation (17).

$$F = ah^{-b} \tag{17}$$

where a and b are constants and h is air film thickness. Peter J. Torvik [14] predicted that the exponent b is about 2; in this paper, the theoretical result is 2.374, and the experimental result is 2.193.

This difference results from the idealization of AFD structure: the theoretical model is only suitable for the case where the air film thickness is thin in comparison to the thickness of the plate; the error is less than 20% when the air film thickness is less than 0.5 *mm*. Once the air film thickness is greater than 0.5 *mm*, the energy dissipated in the fluid decreases; however the material damping may stand out to dissipate the vibration energy which is not involved in the theoretical analysis of this paper.

5.2. Effect of Thin Skin Thickness on Damping Ratio. The AFD structure is designed as 0.125 *mm* thick and installed in Position 1; the thin skin thickness varies from 0.1 *mm* to 0.3 *mm* with an interval of 0.025 *mm*. The effect of thin skin thickness on AFD's damping ratio is shown in Figure 9;

Table 2: Comparison of vibration frequency.

Vibration mode/Plate type	Theoretical results (*Hz*)	Experimental results (*Hz*)	Error (%)
1/Solid plate	59.7	64	6.75
1/AFD plate	64.1	65	1.38
2/Solid plate	379	390	2.82
2/AFD plate	410	406	0.98

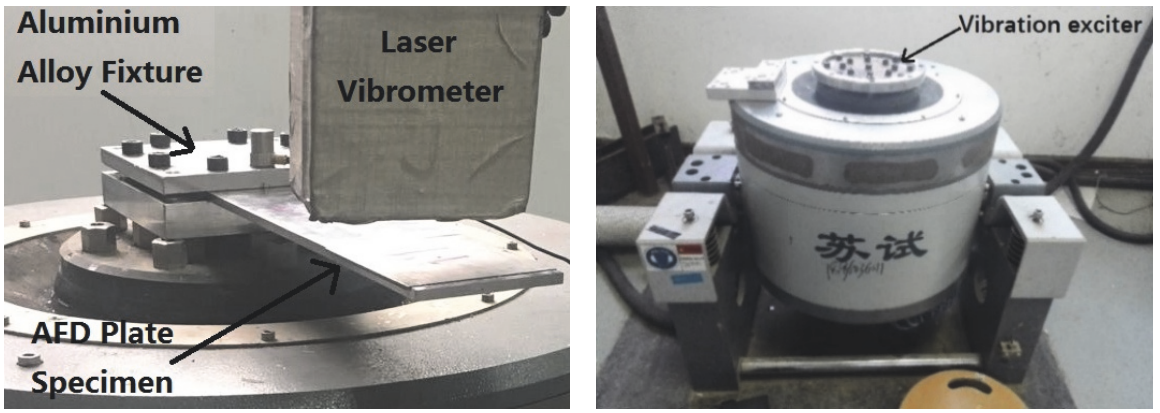

(a) Laser vibrometer system (b) Vibration exciter

Figure 4: Vibration test system.

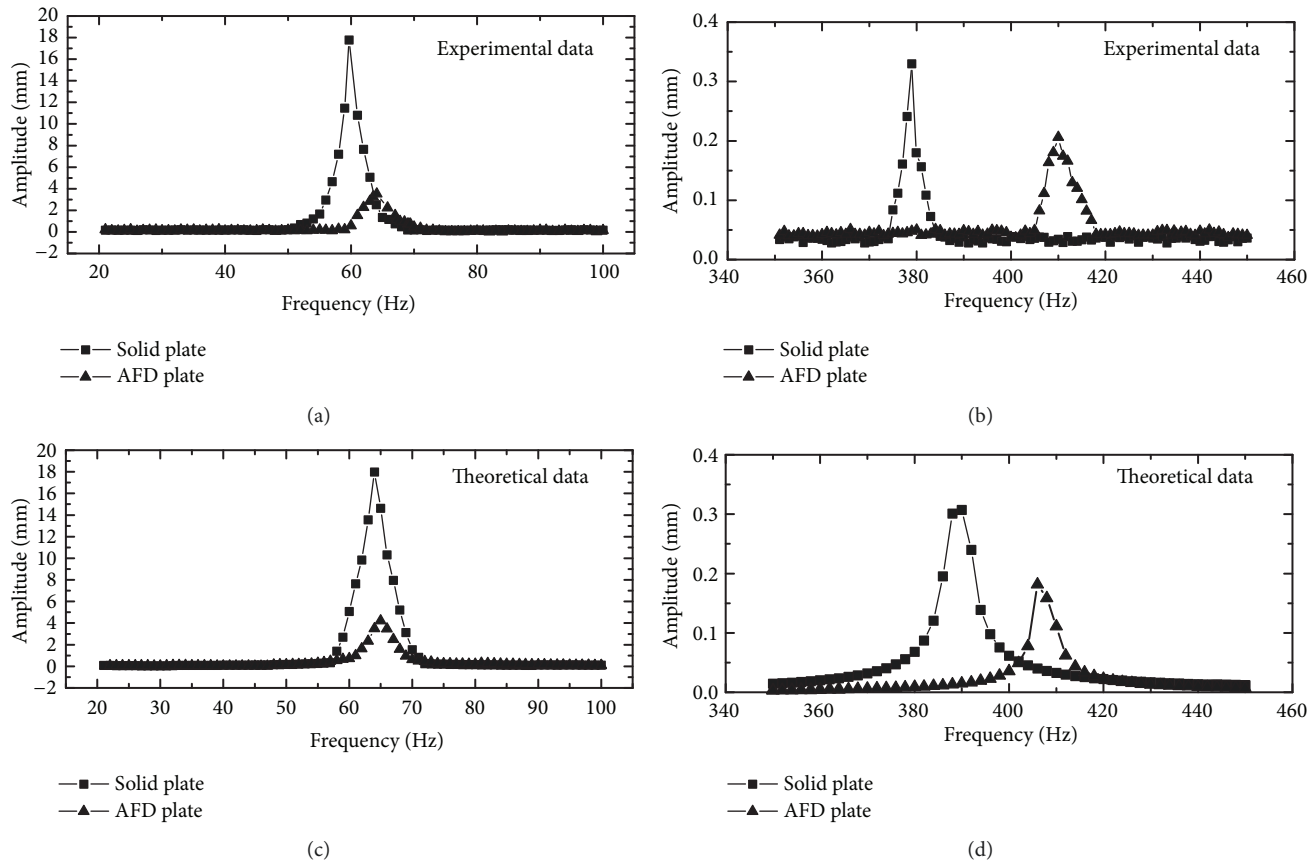

Figure 5: Curve of amplitude of solid plate and AFD plate: (a) and (b) are experimental data; (c) and (d) are theoretical data.

Table 3: Comparison of vibration frequency-amplitude.

Plate type	Frequency ratio	Amplitude (*mm*)	Vibration suppression rate (%)
Solid plate	1	17.771	- - - - - -
Position 1	1.02	3.519	80.198
Position 2	1.34	4.948	72.157
Position 3	1.38	3.879	78.172

Table 4: Vibration information at different air film length.

Plate type	Frequency ratio	Amplitude (*mm*)	Vibration suppression rate (%)
Solid plate	1	17.771	- - - - -
AF 60 *mm*	1.02	7.858	55.782
AF 80 *mm*	1.22	3.519	80.198
AF 100 *mm*	1.16	6.343	64.307

Table 5: Vibration information at different AF thickness.

AF thickness (*mm*)	Theoretical damping ratio	Experimental damping ratio	Error (%)
0.125	0.633	0.55	15.09
0.15	0.48	0.41	18.29
0.2	0.25	0.21	19.05
0.25	0.13	0.12	8.33
0.5	0.022	0.026	15.38
0.75	0.0094	0.012	21.67
1	0.005	0.0067	25.37

Table 6: Damping ratio at different thin skin thickness.

Thin skin thickness (mm)	Theoretical damping ratio	Experimental damping ratio	Error (%)
0.1	0.4	0.35	14.29
0.125	0.415	0.41	12.20
0.15	0.55	0.5	10.00
0.175	0.546	0.523	4.40
0.2	0.6	0.57	5.26
0.225	0.633	0.55	15.09
0.25	0.623	0.525	18.67
0.275	0.586	0.452	25.66
0.3	0.539	0.42	28.33

the theoretical damping ratio is then compared with the experimental damping ratio in Table 5.

The damping ratio increases to a top value and then decreases, and there is obviously an optimal thickness for the thin skin. From Table 6, the damping ratio reaches a top value when the thin skin thickness is 0.15 *mm* ~ 0.25 *mm*. The Levenberg-Marquardt algorithm is applied again for the nonlinear fitting of the data in Table 6 for further analysis.

It is found that the relationship between damping ratio and thin skin thickness conforms to Gaussian equation (18).

$$F = A \exp\left[\frac{-1}{2}\left(\frac{h - h_c}{W}\right)^2\right] \tag{18}$$

where h is the thin skin thickness, h_c is the thickness corresponding to the maximum damping ratio, and W is the standard deviation of the data. In theoretical calculation, h_c=0.227 *mm*, while h_c=0.211 *mm* in experimental analysis. This difference leads to a sharp decrease of the experimental results as the thin skin thickness increases above 0.25 *mm*. Through the analysis of the simplified model, its energy dissipation effect becomes stronger as the frequency of the thin skin is close to the resonance frequency of plate, and the damping effect of the AFD is weakened when the thickness of thin skin increases (its mass increases as well). The mechanism of tuning the vibrating plate is consistent with the mechanism of tuned mass damping [14, 15]; however the

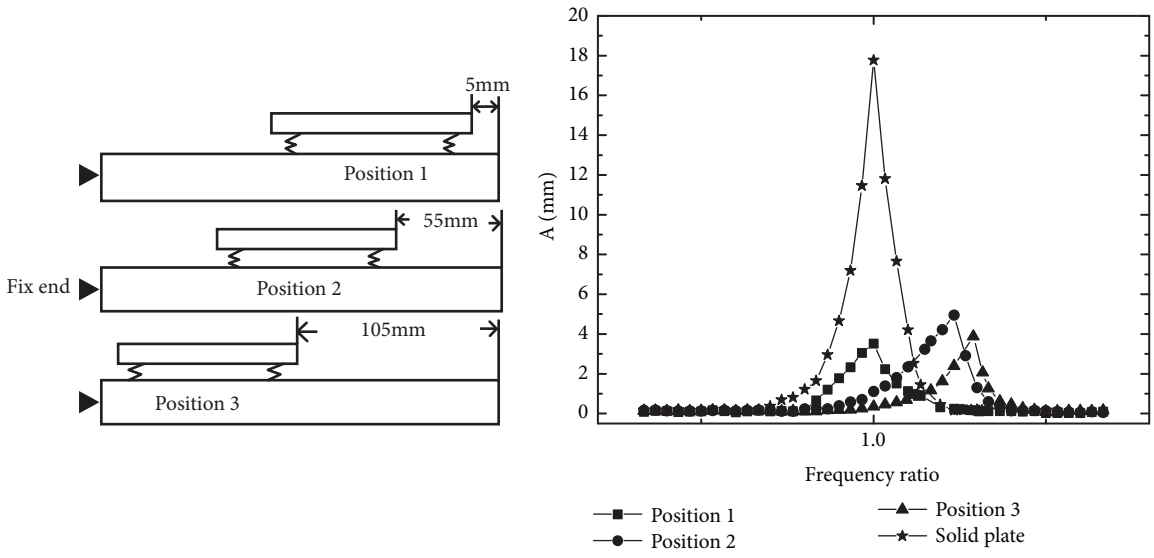

(a) Installation position of thin skin

(b) Effect on amplitude of installation position

Figure 6

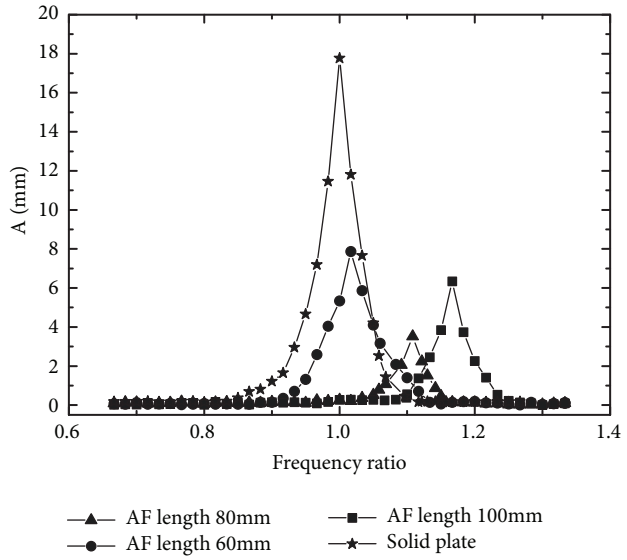

Figure 7: Vibration amplitude of AFD with different air film lengths.

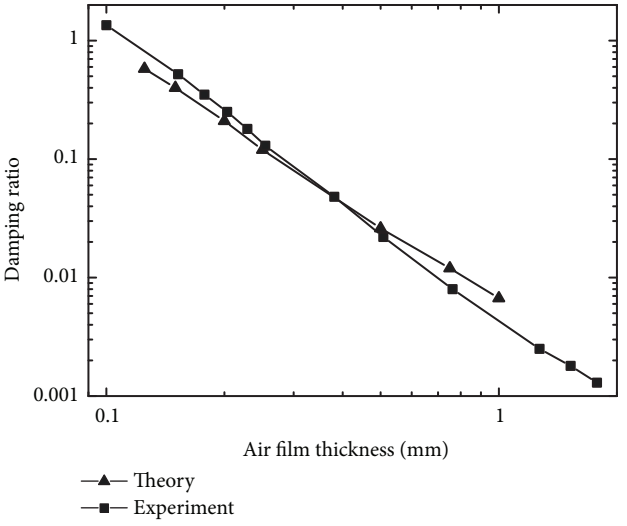

Figure 8: Damping ratio of AFD at different air film thickness.

mechanism is more complicated and requires more in-depth theoretical research.

6. Conclusions

Through the theoretical and experimental research of the AFD structure, the following conclusions are obtained:

(1) The theoretical model established in this paper consists with the experimental analysis as the fluid motion in the air film is considered to deduce the energy dissipation equation of AFD system.

(2) Both theoretical and experimental analyses show that AFD has good suppressing performance on the vibration of the plate specimen in the first two vibration modes.

(3) The structural parameters of the air film, such as the length, installation position, thickness of air film, and thin skin thickness, are key parameters that affect the vibration suppression effect. There is an optimum air film length, and the AFD should be installed at the position where vibration response is maximum; the relationship between damping ratio and air film thickness conforms with the negative exponential function, and the relationship between damping ratio and thin skin thickness confirms the Gauss function.

(4) The resonance frequency of AFD plates shifts in the experiments, and the material damping could be further researched

Data Availability

The data used to support the findings of this study are available from the corresponding author upon request.

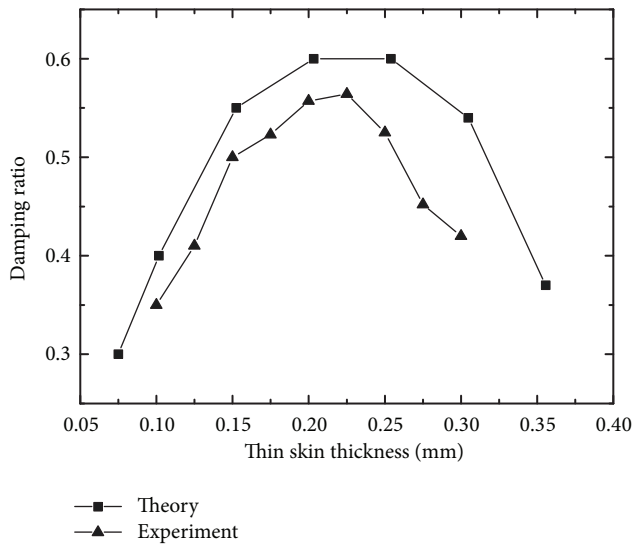

Figure 9: Effect of thin skin thickness on its damping ratio.

Conflicts of Interest

The authors declare that they have no conflicts of interest.

Acknowledgments

This work was financially supported by project "Research on Reliability Design Assurance Technology of Civil Aircraft for Operational Requirements (Project No: MJ-2016-J-91)."

References

[1] C. Zhanyun and J. Liuzhou, "Aero engine strength design and test manual: blade strength and vibration calculation," in *The Third Institute of Machinery Industry*, pp. 34–68, Beijing, China, 2001.

[2] T. Lewis and K. Notestine, "Air film damping for turbine engine applications," in *Proceedings of the 9th High Cycle Fatigue (HCF) Conference*, Pinehurst, North Carolina, USA, 2004.

[3] M. Inoue, I. Yokomichi, and K. Hiraki, "Particle damping with granular materials for multi degree of freedom system," *Shock and Vibration*, vol. 18, no. 1-2, Article ID 309682, pp. 245–256, 2011.

[4] E. E. Ungar and J. R. Carbonell, "On panel vibration due to to structural joints," *AIAA*, vol. 4, pp. 1385–1390, 1966.

[5] G. Maidanik, "Energy dissipation associated with gas-pumping in structural joints," *The Journal of the Acoustical Society of America*, vol. 40, no. 5, pp. 1064–1072, 1966.

[6] M. Fox and P. Whitton, "The damping of structural vibration by thin gas films," *Journal of Sound and Vibration*, vol. 73, no. 2, pp. 279–295, 1980.

[7] L. Chow and R. Pinnington, "Practical industrial method of increasing structural damping in machinery, I: Squeeze-film damping with air," *Journal of Sound and Vibration*, vol. 118, no. 1, pp. 123–139, 1987.

[8] L. Chow and R. Pinnington, "Practical industrial method of increasing structural damping in machinery, II: Squeeze-film damping with liquids," *Journal of Sound and Vibration*, vol. 128, no. 2, pp. 333–347, 1989.

[9] A. Trochidis, "Körperschalldampfung mittels gas-order flüssigkeitsschichten (vibration damping due to air or liquid layers," *Acta Acustica United with Acustica*, vol. 51, pp. 201–212, 1989.

[10] T. Lewis, D. I. G. Jones, and C. Michael, "Partial coverage air film damping of cantilever plates," *Journal of Sound and Vibration*, vol. 208, no. 5, pp. 869–875, 1997.

[11] T. Lewis, K. Notestine, D. Jones, S. Halfhill, M. Parin, and F. Lieghley, "Air film damping for turbine engine applications," in *Proceedings of the 10th High Cycle Fatigue (HCF) Conference*, pp. 8–11, 2005.

[12] T. Lewis, K. Notestine, D. I. G. Jones, M. McCormack, and D. Vetters, "Recent advances in air film damping for gas turbine applications," in *Proceedings of the 8th High Cycle Fatigue (HCF) Conference*, pp. 14–16, Monterey, Canada, 2003.

[13] T. Lewis, "Air film damping," in *Proceedings of the Presentation, AT/GUIDe Meeting*, Duke University, 2000.

[14] P. J. Torvik, "The dynamics of the air film damper," in *Proceedings of the 9th High Cycle Fatigue (HCF) Conference*, vol. 5, pp. 28–31, 2004.

[15] D.-Y. Zhang, Y.-F. He, L.-L. Chen, Y.-H. Ma, and J. Hong, "Theoretical investigation on vibration characteristics of structure with air film damper," *Journal of Aerospace Power*, vol. 31, no. 2, pp. 282–288, 2016.

[16] R. M. Mathison, M. G. Dunn, M. M. Weaver, and A. Dushko, "Measurement of air film damping effectiveness," *Journal of Turbomachinery*, vol. 127, no. 3, pp. 557–563, 2005.

[17] S. Rothberg, M. Allen, P. Castellini et al., "An international review of laser Doppler vibrometry: Making light work of vibration measurement," *Optics and Lasers in Engineering*, vol. 99, pp. 11–22, 2017.

[18] S. Chakraverty, *Vibration of Plates*, CRC Press, New York, NY, USA, 2009.

[19] W. Leissa A, *Vibration of Plates*, Ohio State University, Columbia, Ga, USA, 2015.

[20] E. de Barros and C. D. Souto, "Evaluation of a vibration text fixture," *International Journal of Acoustics and Vibration*, vol. 22, 2017.

[21] L. P. Beverlin, D. K. Rollins, N. Vyas, and D. Andre, "An algorithm for optimally fitting a wiener model," *Mathematical Problems in Engineering*, vol. 2011, Article ID 570509, 15 pages, 2011.